Mon. Not. R. Astron. Soc. **000**, 1–6 (2008) Printed 29 August 2008 (MN LATEX style file v2.2)

On the Anomalous Silicate Emission Features of AGNs: A Possible Interpretation Based on Porous Dust

M.P. Li[1], Q.J. Shi[2] and Aigen Li[1] ⋆
[1] *Department of Physics & Astronomy, University of Missouri, Columbia, MO 65211, USA*
[2] *Department of Science and Engineering of Shuda College, Hunan Normal University, Changsha, Hunan 410081, China*

Received date / Accepted date

ABSTRACT
The recent *Spitzer* detections of the 9.7 μm Si–O silicate emission in type 1 AGNs provide support for the AGN unification scheme. The properties of the silicate dust are of key importance to understanding the physical, chemical and evolutionary properties of the obscuring dusty torus around AGNs. Compared to that of the Galactic interstellar medium (ISM), the 10 μm silicate emission profile of type 1 AGNs is broadened and has a clear shift of peak position to longer wavelengths. In literature this is generally interpreted as an indication of the deviations of the silicate composition, size, and degree of crystallization of AGNs from that of the Galactic ISM. In this *Letter* we show that the observed peak shift and profile broadening of the 9.7 μm silicate emission feature can be explained in terms of porous composite dust consisting of ordinary interstellar amorphous silicate, amorphous carbon and vacuum. Porous dust is naturally expected in the dense circumnuclear region around AGNs, as a consequence of grain coagulation.

Key words: galaxies: active – galaxies: ISM : dust – infrared: galaxies

1 INTRODUCTION

Dust is the cornerstone of the unification theory of active galactic nuclei (AGNs). This theory proposes that all AGNs are essentially "born equal" – all types of AGNs are surrounded by an optically thick dust torus and are basically the same object but viewed from different lines of sight (see e.g. Antonucci 1993; Urry & Padovani 1995): type 1 AGNs, which always display broad hydrogen emission lines in the optical and have no obvious obscuring effect, are viewed face-on which allows a direct view of the central nuclei, while type 2 AGNs are viewed edge-on with most of the central engine and broad line regions being hidden by the obscuring dust.

Silicate dust, a major solid species in the Galactic interstellar medium (ISM) as revealed by the strong 9.7 μm and 18 μm bands (respectively ascribed to the Si–O stretching and O–Si–O bending modes in some form of silicate material, e.g. olivine $Mg_{2x}Fe_{2-2x}SiO_4$), has also been detected in AGNs both in *emission* and in *absorption* (see Li 2007 for a review).

The first detection of the silicate *absorption* feature in AGNs was made at 9.7 μm for the prototypical Seyfert 2 galaxy NGC 1068 (Rieke & Low 1975; Kleinmann et al. 1976), indicating the presence of a large column of silicate dust in the line-of-sight to the nucleus. It is known now that most of the type 2 AGNs display silicate *absorption* bands (e.g. see Roche et al. 1991, Siebenmorgen et al. 2004, Hao et al. 2007, Spoon et al. 2007, Roche et al. 2007) which is expected from the AGN unified theory – for a centrally heated optically thick torus viewed edge-on, the silicate features should be in absorption.

For type 1 AGNs viewed face-on, one would expect to see the silicate features in *emission* since the silicate dust in the surface of the inner torus wall will be heated to temperatures of several hundred kelvin to ~ 1000 K by the radiation from the central engine, allowing for a direct detection of the 9.7 μm and 18 μm silicate bands emitted from this hot dust. However, their detection has only very recently been reported in a number of type 1 AGNs covering a broad luminosity range, thanks to *Spitzer* (Hao et al. 2005, Siebenmorgen et al. 2005, Sturm et al. 2005, Weedman et al. 2005, Shi et al. 2006, Schweitzer et al. 2008). It is worth noting that the silicate emission features have recently also been detected in type 2 QSOs (Sturm et al. 2006, Teplitz et al. 2006).

Compared to that of the Galactic ISM, the 9.7 μm silicate emission profiles of some AGNs appear "anomalous". As illustrated in Figure 1, both quasars (high luminosity counterparts of Seyfert 1 galaxies; Hao et al. 2005, Siebenmorgen et al. 2005) and the low-luminosity AGN NGC 3998 (Sturm et al. 2005) exhibit silicate emission peaks at a

⋆ E-mail: limo@missouri.edu, qingjiongshi@gmail.com, lia@missouri.edu

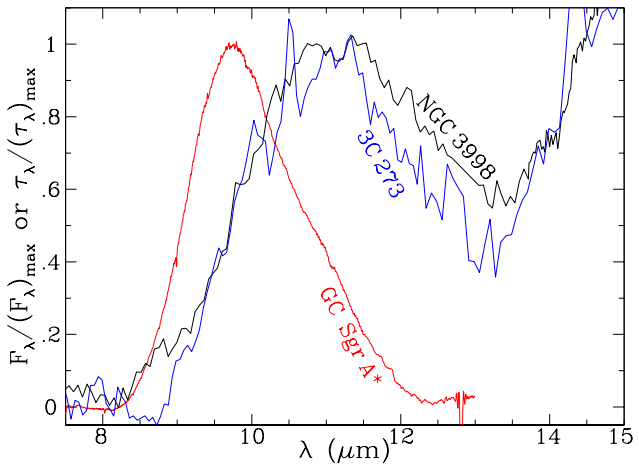

Figure 1. Comparison of the silicate emission features of the quasar 3C 273 (Hao et al. 2005) and the low-luminosity AGN NGC 3998 (Sturm et al. 2005) with the silicate absorption feature of the ISM toward the Galactic center object Sgr A* (Kemper et al. 2004). Most notably is the long wavelength shift of the peak positions of 3C 273 and NGC 3998 in comparison with the ISM profile. All profiles are normalized to their peak values.

much longer wavelength ($\sim$10–11.5 μm), inconsistent with the "standard" silicate ISM dust (which peaks at $\sim$9.7 μm). The 9.7 μm feature of NGC 3998 is also much broader than that of the Galactic ISM (Sturm et al. 2005).[1]

The deviations of the silicate emission profiles of type 1 AGNs from that of the Galactic ISM dust are generally interpreted as an indication of the differences between AGNs and the Galactic ISM in the composition, size distribution, and degree of crystallization of the silicate dust (Sturm et al. 2005). However, we show in this *Letter* that the observed peak shift and profile broadening of the 9.7 μm silicate emission features of AGNs can be explained in terms of porous composite dust consisting of ordinary interstellar amorphous silicate, amorphous carbon[2] and vacuum, without invoking an exotic dust composition or size distribution. In the dense circumnuclear region around AGNs, a porous structure is naturally expected for the dust formed through the coagulation of small silicate and carbonaceous grains.

2 MODEL OF POROUS COMPOSITE DUST

To model the porous composite dust, we adopt the multi-layered sphere model originally developed by Voshchinnikov & Mathis (1999). This model assumes that the dust consists of many concentric spherical layers of different types of materials. Each of the material has a given volume fraction. Voshchinnikov et al. (2005, 2006) demonstrated that the optical properties of porous dust calculated from the multi-layered sphere model is in close agreement with that from the discrete dipole approximation (DDA; Draine 1988).While the DDA method is computationally very time-consuming, the multi-layered sphere model is computationally much less demanding but still accurate for computing the integral scattering characteristics (e.g. extinction, scattering, absorption cross sections, albedo and asymmetry parameter) and becomes a robust tool to model the optical properties of composite dust with a porous structure.

We consider three types of dust materials in the model: amorphous silicate with olivine composition ($MgFeSiO_4$), amorphous carbon, and vacuum. We take the optical constants of amorphous olivine $MgFeSiO_4$ from Dorschner et al. (1995); for amorphous carbon, we take those of Rouleau & Martin (1991).

In the multi-layered sphere model, we need to specify (1) $n_{\rm layer}$ – the number of layers; (2) P – the dust porosity (i.e. the volume fraction of vacuum in a fluffy porous grain); (3) $m_{\rm carb}/m_{\rm sil}$ – the mass ratio of amorphous carbon to amorphous silicate in a grain; (4) $r_{\rm compact}$ – the radius of the mass-equivalent compact sphere. Voshchinnikov et al. (2005) found that the optical properties of layered dust are independent of the number and position of layers when the number of layers $n_{\rm layer}$ exceeds 15. We therefore take $n_{\rm layer} = 18$.[3] We consider a range of porosities, with P ranging from $P = 0$ (compact dust) to $P = 0.9$. We take the mass ratio of amorphous carbon to amorphous silicate to be $m_{\rm carb}/m_{\rm sil} = 0.7$ which is estimated from the cosmic abundance constraints (see Li & Lunine 2003).[4] We take the radius of the mass-equivalent compact spherical grain to be $r_{\rm compact} = 0.1\,\mu$m, a typical size for interstellar dust.[5] For a porous dust of porosity P with the same mass as that of the compact dust of radius $r_{\rm compact}$, its radius is $r_{\rm porous} = r_{\rm compact}/(1-P)^{1/3}$. For a given $r_{\rm compact}$, $r_{\rm porous}$ moderately increases with P.

3 RESULTS

Using the computational techniques of the multi-layered sphere model of Voshchinnikov & Mathis (1999) and assuming $n_{\rm layer} = 18$, $m_{\rm carb}/m_{\rm sil} = 0.7$, and $r_{\rm compact} = 0.1\,\mu$m (see §2), we calculate the absorption efficiency factors $Q_{\rm abs}(\lambda)$ for porous composite dust of a range of porosities. We show in Figure 2 the 8–13 μm absorption efficiency $Q_{\rm abs}(\lambda)$ calculated for porous composite dust con-

[1] We should note that the width of the interstellar 9.7 μm Si–O absorption feature is not universal, but varies from one sightline to another (see Draine 2003). Generally speaking, it is relatively narrow in diffuse clouds and broad in molecular clouds (Bowey et al. 1998). In contrast, its peak wavelength is relatively stable.

[2] There must exist a population of carbonaceous dust in the AGN torus, as revealed by the detection of the 3.4 μm absorption feature, attributed to the C–H stretching mode in saturated aliphatic hydrocarbon dust (see Li 2007 for a review). Whether the bulk form of the carbonaceous component in AGNs is amorphous carbon or hydrogenated amorphous carbon is not clear.

[3] This means that each layered dust has 6 shells, and every shell has 3 layers consisting of amorphous silicate, amorphous carbon and vacuum.

[4] With the mass density of amorphous silicate $\rho_{\rm sil} = 3.5\,{\rm g\,cm^{-3}}$ and the mass density of amorphous carbon $\rho_{\rm carb} = 1.8\,{\rm g\,cm^{-3}}$, this mass ratio corresponds to a volume ratio of $V_{\rm carb}/V_{\rm sil} \approx 1.4$.

[5] With a larger $r_{\rm compact}$, the peak wavelength $\lambda_{\rm peak}$ and width of the 9.7 μm Si–O band will be further red-shifted and broadened. But as $r_{\rm compact}$ exceeds $\sim$0.5 μm, the 9.7 μm Si–O feature fades away for porous dust with $P > 0.5$.

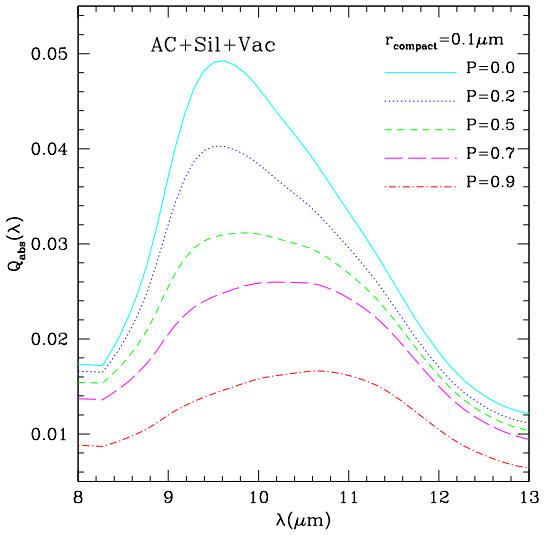

Figure 2. 8–13 μm absorption efficiencies $Q_{\rm abs}(\lambda)$ of porous composite grains consisting of amorphous silicate, amorphous carbon and vacuum with $P = 0, 0.2, 0.5, 0.7, 0.9$. Note the progressive broadening of the 9.7 μm Si–O feature and the progressive shift to longer wavelengths of its peak position with the increase of the dust porosity P.

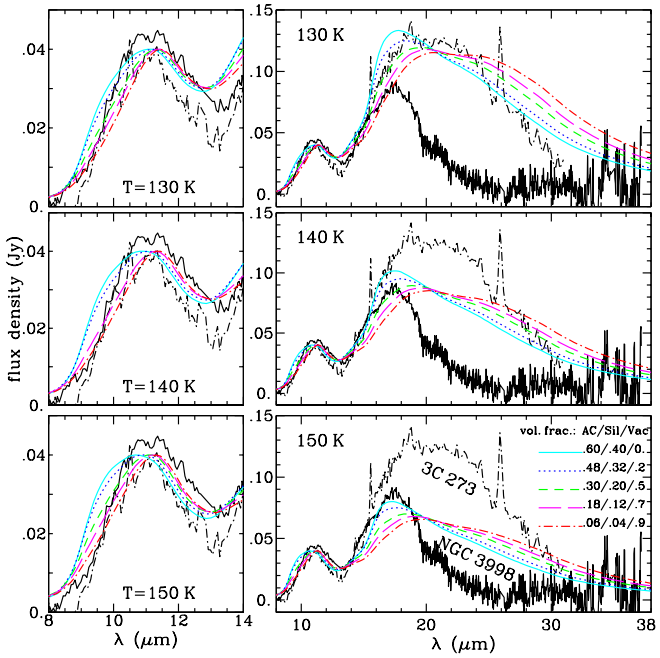

Figure 3. Comparison of the silicate emission spectra calculated from the porous composite dust model with that observed in 3C 273 (a bright quasar) and NGC 3998 (a low luminosity galaxy). The model emission spectra are obtained by folding the absorption efficiencies $Q_{\rm abs}(\lambda)$ of porous composite dust (see Fig. 2) with a Planck function at temperature T and then scaled to the flux densities of the 9.7 μm features of 3C 273 and NGC 3998.

sisting of amorphous silicate, amorphous carbon and vacuum with $P = 0, 0.2, 0.5, 0.7, 0.9$. With $r_{\rm compact} = 0.1\,\mu$m, the radius of the porous dust corresponds to $r_{\rm porous} \approx 0.108, 0.126, 0.149, 0.215\,\mu$m for $P = 0.2, 0.5, 0.7, 0.9$, respectively (for compact dust, the 9.7 μm silicate absorption profiles are essentially identical for grains of radii $r = 0.1$, 0.108, 0.126, 0.149, 0.215 μm, as expected since they are in the Rayleigh regime at $\lambda = 10\,\mu$m). Most notably in Figure 2 are the progressive broadening of the 9.7 μm Si–O feature and the progressive shift to longer wavelengths of the peak position of this feature as the dust porosity P increases: while the silicate feature peaks at $\sim 9.6\,\mu$m and has a FWHM (full width half maximum) $\sim 2.1\,\mu$m for compact dust ($P = 0$), its peak shifts to $\sim 10.6\,\mu$m and its FWHM is broadened to $\sim 2.8\,\mu$m for very fluffy dust ($P = 0.9$); the 9.7 μm Si–O feature is significantly flattened as the porosity increases from $P = 0$ to $P = 0.9$.

In order to have a direct comparison between the porous dust model with the "anomalous" silicate *emission* features observed in AGNs, we first multiply the calculated absorption efficiency $Q_{\rm abs}(\lambda)$ with a Planck function $B_\lambda(T)$ at temperature T. For a given T we further multiply the product of $Q_{\rm abs}(\lambda)$ and $B_\lambda(T)$ with a constant to force the model to fit the observed flux density of the 9.7 μm feature. This approach is valid if the silicate feature emitting regions are optically thin.[6]

We take 3C 273 (a bright quasar; Hao et al. 2005) and NGC 3998 (a low luminosity AGN whose luminosity is $\sim$4–5 orders of magnitude below those of quasars; Sturm et al. 2005) as two test cases. While their 9.7 μm Si–O features are virtually identical (see Fig. 1), at the 18 μm O–Si–O feature region they deviate significantly from each other (see Fig. 3).

As shown in Figure 3, with $T \sim 120$–220 K, the porous composite dust model fits the broadened and long wavelength-shifted 9.7 μm feature of 3C 273 and NGC 3998 reasonably well. The required temperature ($T \sim 120$–220 K) is consistent with that constrained by Hao et al. (2005) and Sturm et al. (2005). With $T = 130$ K the model (with $P \leq 0.2$) is also in a reasonably good agreement with the long-wavelength wing of the 18 μm feature of 3C 273. It is more challenging to fit that of NGC 3998 which is much weaker than that of 3C 273 and peaks at $\sim 18.5\,\mu$m (while the "18 μm" O–Si–O feature of 3C 273 peaks at $\sim 20\,\mu$m).[7]

[6] The optical thin assumption is reasonable if the silicate emission mainly comes from the unblocked surface layer of the inner torus wall. However, the inferred temperatures ($T < 220$ K) for 3C 273 and NGC 3998 (see Figs. 3,4) are much lower than that expected for the dust near the surface of the inner torus wall where the temperature of silicate dust should be close to its sublimation temperature ($\sim$800–1500 K; Kimura et al. 2002). Sturm et al. (2005) suggested that this emission may actually originate from the extended narrow-line regions (NLRs) which are beyond the torus. The NLR origin of the silicate emission is consistent with the detection of silicate emission in type 2 QSOs (see Efstathiou 2006, Marshall et al. 2007, Schweitzer et al. 2008). Alternatively, the silicate emission could originate from the inner regions of the torus provided that the torus is clumpy so that the light from the central engine is substantially attenuated (e.g. see Levenson et al. 2007, Nenkova et al. 2002, 2008).

[7] It is possible that the composition of the silicate dust in NGC 3998 may differ from that in 3C 273, suggesting that there might be significant environmental variations (after all, NGC 3998 is a LINER galaxy with an AGN luminosity $\sim 1.7 \times 10^4$ times

Qualitatively speaking, one requires a higher T and a high porosity ($P \geq 0.7$) to fit the 18 μm feature of NGC 3998.[8] We should emphasize that the major purpose of this work is not to provide a detailed modeling of the silicate emission spectra of 3C 273 and NGC 3998, but to put forward a hypothesis that the peak redshift and profile broadening of the 9.7 μm Si–O emission features observed in some AGNs could result from the porous structure of the dust.

In the Hao et al. (2005) sample, four quasars (among the five PG quasars displaying the 9.7 μm and 18 μm silicate emission features, apart from 3C 273) exhibit an 18 μm O–Si–O emission feature intermediate between that of NGC 3998 and that of 3C 273 (while their 9.7 μm features are all similar). As can be seen in Figure 3, the porous composite dust model with $T \sim 130$–150 K should be able to simultaneously fit both the 9.7 μm features and the 18 μm features of those quasars.

4 DISCUSSION

It is well-known theoretically that as the size of a silicate grain increases, the 9.7 μm Si–O feature becomes wider with its peak shifted to longer wavelengths (see Fig. 9 of Dorschner et al. 1995, Fig. 1 of Voshchinnikov & Henning 2008). But for compact silicate spheres to have its 9.7 μm Si–O feature peaking at $\lambda_{\rm peak} > 10.5\,\mu$m, their size needs to exceed $\sim 2\,\mu$m. However, for these large grains the 9.7 μm Si–O feature fades away (see Fig. 6 of Greenberg 1996, Fig. 1 of Voshchinnikov & Henning 2008). Therefore, it is difficult to account for the "anomalous" silicate emission features of AGNs just in terms of an increase in grain size.

A non-spherical grain shape or shape distribution can also broaden the 9.7 μm Si–O feature and red-shift its peak wavelength (see Li 2008). But to account for the peak wavelengths of $\lambda_{\rm peak} \sim 10$–$11.5\,\mu$m observed in some AGNs, the dust has to be extremely elongated which is unrealistic (e.g. spheroidal dust needs to have an elongation >6).

The peak wavelength of the 9.7 μm Si–O feature also depends on the silicate mineralogy. But we are not aware of any amorphous silicate species that could give rise to a Si–O feature peaking at $\lambda > 10\,\mu$m.

Crystalline olivine has its Si–O feature peaks at $\sim 11.2\,\mu$m (see Yamamoto et al. 2008). But this feature is too sharp compared to the broad Si–O emission features of AGNs. Within the signal-to-noise ratio limits, we see no clear evidence for crystalline silicates in 3C 273 and NGC 3998 (see Fig. 1). So far, the detection of crystalline silicate dust in AGNs has only been reported in the BAL (broad absorption line) quasar PG 2112+059 (Markwick-Kemper et al. 2007).[9] The 9.7 μm Si–O feature emission features of the protoplanetary disks around T Tauri and Herbig Ae/Be stars are often also much broader than that of the ISM (e.g. see Bouwman et al. 2001, Forrest et al. 2004). This is usually interpreted as an indicator of grain growth (e.g. see Natta et al. 2007). The porous composite dust model was recently used by Voshchinnikov & Henning (2008) to demonstrate that a similar behavior of the feature shape occurs when the porosity of fluffy dust varies. Krügel & Siebenmorgen (1994) have also demonstrated that a porous structure results in the broadening, weakening and redshifting of the 9.7 μm Si–O feature. Fluffy dust aggregates are also naturally expected in protoplanetary disks as a result of grain coagulation.

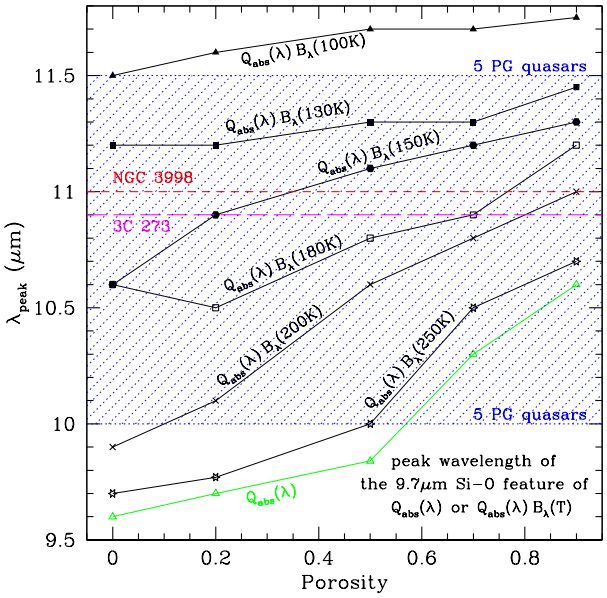

Figure 4. Peak wavelengths of the "9.7 μm" Si–O silicate features of $Q_{\rm abs}(\lambda)$ or $Q_{\rm abs}(\lambda)\,B_\lambda(T)$ as a function of dust porosity for a range of temperatures $T = 100$, 130, 150, 180, 200 and 250 K. Also plotted are the peak wavelengths of the 9.7 μm feature of NGC 3998 and 3C 273. The shaded area plots the range of the peak wavelengths of the 9.7 μm Si–O emission features of the five quasars observed by Hao et al. (2005): $10\,\mu{\rm m} \leq \lambda_{\rm peak} \leq 11.5\,\mu{\rm m}$.

We plot in Figure 4 as a function of porosity P the peak wavelengths $\lambda_{\rm peak}$ of the 9.7 μm Si–O feature of the absorption efficiency profiles $Q_{\rm abs}(\lambda)$ and the emission profiles obtained by folding $Q_{\rm abs}(\lambda)$ with the Planck function $B_\lambda(T)$ at various temperatures. It is seen that for 3C 273 and NGC 3998, to account for the observed $\lambda_{\rm peak} \approx 10.6\,\mu$m, one requires either cool dust (with $T \sim 140$–150 K) with a low porosity ($P < 0.3$), or warm dust (with $T \sim 170$–220 K) with a high porosity ($P > 0.6$). The 18 μm O–Si–O emis-

below that of the bright quasar 3C 373; it is therefore possible that the silicate dust in NGC 3998 subjects to different degrees of processing compared to that in 3C 273.) As shown experimentally in Dorschner et al. (1995), the peak wavelength, width and strength of the "18 μm" O–Si–O feature (relative to the 9.7 μm Si–O feature) vary among silicate minerals of different composition. The optical constants of amorphous olivine $MgFeSiO_4$ chosen here may not be the most suitable ones for NGC 3998 (e.g. the fast declining red wing of the 18 μm feature may suggest the presence of clino-pyroxenes [Wooden et al. 1999]).

[8] One may ask why our models imply that the dust in 3C 273 is cooler than the dust in NGC 3998 while 3C 273 is much more luminous. A plausible answer is that the silicate emission actually originates from the NLRs far away from the central heating regions or from a clumpy, attenuated torus.

[9] Spoon et al. (2006) reported firstly the detection of narrow absorption features of crystalline silicates in ultraluminous IR galaxies (ULIRGs).

sion feature further constrains that cool dust is preferred in 3C 273 while NGC 3998 appears to favour warm dust.

Also seen in Figure 4 is that the range of the peak wavelengths $10\,\mu\mathrm{m} \leq \lambda_{\mathrm{peak}} \leq 11.5\,\mu\mathrm{m}$ of the $9.7\,\mu$m Si–O emission features of the five PG quasars of Hao et al. (2005) falls within the predictions of the porous composite dust model. This indicates that the long-wavelength shifted $9.7\,\mu$m Si–O features of these quasars can be accounted for by the combined effects of porosity and temperature (i.e. either highly porous warm dust or cold dust with a lower porosity). The $18\,\mu$m O–Si–O emission feature will allow us to break this degeneracy. Finally, for those AGNs whose $9.7\,\mu$m Si–O absorption or emission features do not exhibit any long-wavelength shift, one may resort to dust with a low porosity $P < 0.3$ (and $T > 220\,\mathrm{K}$ if they are in emission).

We should stress that although the combined effects of porosity and temperature suffice by themselves to explain the general trend of broadening the $9.7\,\mu$m Si–O emission features of AGNs and shifting their peak wavelengths to longer wavelengths, we by no means exclude the effects of other factors such as grain size,[10] shape, and mineralogy. It is very likely that all these factors act together to produce the anomalous silicate emission features seen in AGNs.

Finally, we emphasize that although a steeply rising (cold) Planck function could redshift the $9.7\,\mu$m Si–O emission feature, the observed shift of the peak wavelength of this emission feature in AGNs cannot be purely a temperature effect since the silicate absorption profiles of some AGNs also appear anomalous; e.g., the "$9.7\,\mu$m" silicate feature of Mkn 231, a peculiar type 1 Seyfert galaxy, is seen in absorption peaking at $\sim 10.5\,\mu$m (Roche et al. 1983); Jaffe et al. (2004) found that the $9.7\,\mu$m silicate absorption spectrum of NGC 1068 shows a relatively flat profile from 8 to $9\,\mu$m and then a sharp drop between 9 and $10\,\mu$m; in comparison, the Galactic silicate absorption profiles begin to drop already at $\sim 8\,\mu$m.

To conclude, we have explored in a quantitative way on the effects of grain porosity on the silicate Si–O stretching feature using the multi-layered sphere model. It is found that the Si–O feature broadens and shifts to longer wavelengths with the increasing of dust porosity. We conclude that the combined effects of dust porosity and cool temperature of $T < 200\,\mathrm{K}$ (which further redshifts the silicate feature) could explain the observed broadening and longer-wavelength shifting of the $9.7\,\mu$m Si–O feature of AGNs.

[10] The grain size effect is probably (at least in part) responsible for the nondetection of the $9.7\,\mu$m and $18\,\mu$m silicate emission features in many type 1 AGNs (e.g. see Hao et al. 2007). The silicate size distribution in some AGNs might be dominated by large grains ($>$ a few μm; see Maiolino et al. 2001a,b) or small silicate grains are depleted (e.g. see Laor & Draine 1993, Granato & Danese 1994). Alternative explanations include sophisticated torus geometries (e.g. tapered disk configurations [Efstathiou & Rowan-Robinson 1995], clumpy torus models [Nenkova et al. 2002, 2008; but see Dullemond & van Bemmel 2005]) and an assumption of strong anisotropy of the source radiation (Manske et al. 1998).

ACKNOWLEDGMENTS

We thank L. Hao and E. Strum for providing us with *Spitzer* IRS spectra of 3C 273 and NGC 3998. We thank L. Hao and R. Siebenmorgen for very helpful comments. ML and AL are supported in part by NASA/HST Theory Programs, and NASA/Spitzer Theory Programs. AL is supported by the NSFC Outstanding Overseas Young Scholarship.

REFERENCES

Antonucci, R. 1993, ARA&A, 31, 473
Bouwman, J., Meeus, G., de Koter, A., Hony, S., Dominik, C., & Waters, L. B. F. M. 2001, A&A, 375, 950
Bowey, J. E., Adamson, A. J., & Whittet, D. C. B. 1998, MNRAS, 298, 131
Dorschner, J., Begemann, B., Henning, Jäger, C., Mutschke, H. 1995, A&A, 300, 503
Draine, B. T. 1988, ApJ, 333, 848
Draine, B. T. 2003, ARA&A, 41, 241
Dullemond, C. P., & van Bemmel, I. M. 2005, A&A, 436, 47
Efstathiou, A. 2006, MNRAS, 371, L70
Efstathiou, A., & Rowan-Robinson, M. 1995, MNRAS, 273, 649
Forrest, W. J., et al. 2004, ApJS, 154, 443
Granato, G. L., & Danese, L. 1994, MNRAS, 268, 235
Greenberg, J. M. 1996 in Cosmic Dust Connection, ed. J.M. Greenberg (Dordrecht: Kluwer), 443
Hao, L., et al. 2005, ApJ, 625, L75
Hao, L., Weedman, D. W., Spoon, H. W. W., Marshall, J. A., Levenson, N. A., Elitzur, M., & Houck, J. R. 2007, ApJ, 655, L77
Jaffe, W., et al. 2004, Nature, 429, 47
Kemper, F., Vriend, W. J., Tielens, A. G. G. M. 2004, ApJ, 609, 826 (Erratum: 2005, ApJ, 633, 534)
Kimura, H., Mann, I., Biesecker, D. A., & Jessberger, E. K. 2002, Icarus, 159, 529
Kleinmann, D.E., Gillett, F.C., & Wright, E.L. 1976, ApJ, 208, 42
Krügel, E., & Siebenmorgen, R. 1994, A&A, 288, 929
Laor, A., & Draine, B. T. 1993, ApJ, 402, 441
Levenson, N. A., et al. 2007, ApJ, 654, L45
Li, A. 2007, in ASP Conf. Ser. 373, The Central Engine of Active Galactic Nuclei, ed. L. C. Ho & J.-M. Wang (San Francisco: ASP), 561
Li, A. 2008, in Small Bodies in Planetary Sciences (Lecture Notes in Physics Series), I. Mann, A. Nakamura, & T. Mukai (eds.), Springer, 167
Li, A., & Lunine, J. I. 2003, 590, 368
Maiolino, R., Marconi, A., Salvati, M., Risaliti, G., Severgnini, P., Oliva, E., La Franca, F., & Vanzi, L. 2001a, A&A, 365, 28
Maiolino, R., Marconi, A., & Oliva, E. 2001b, A&A, 365, 37
Manske, V., Henning, Th., & Men'shchikov, A.B. 1998, A&A, 331, 52
Markwick-Kemper, F., Gallagher, S. C., Hines, D. C., & Bouwman, J. 2007, ApJ, 668, L107
Marshall, J.A., Herter, T.L., Armus, L., Charmandaris, V., Spoon, H.W.W., Bernard-Salas, J., & Houck, J.R. 2007, ApJ, 670, 129
Natta, A., Testi, L., Calvet, N., Henning, T., Waters, R., & Wilner, D. 2007, in Protostars and Planets V, ed. B. Reipurth, D. Jewitt, & K. Keil (Tucson: Univ. Arizona Press), 767
Nenkova, M., Ivezic, Z., & Elitzur, M. 2002, ApJ, 570, L9
Nenkova, M., Sirocky, M. M., Nikutta, R., Ivezic, Z., & Elitzur, M. 2008, ApJ, in press
Rieke, G.H., & Low, F.J. 1975, ApJ, 199, L13
Roche, P.F., Aitken, D.K., & Whitmore, B. 1983, MNRAS, 205, P21

Roche, P. F., Aitken, D. K., & Smith, C. H. 1991, MNRAS, 252, 282
Roche, P.F., Packham, C., Aitken, D.K., & Mason, R.E. 2007, MNRAS, 375, 99
Rouleau, F., & Martin, P. G. 1991, ApJ, 377, 526
Schweitzer, M., et al. 2008, ApJ, 679, 101
Shi, Y., et al. 2006, ApJ, 653, 127
Siebenmorgen, R., Krügel, E., & Spoon, H. W. W. 2004, A&A, 414, 123
Siebenmorgen, R., Haas, M., Krügel, E., & Schulz, B. 2005, A&A, 436, L5
Spoon, H.W.W., et al. 2006, ApJ, 638, 759
Spoon, H. W. W., Marshall, J. A., Houck, J. R., Elitzur, M., Hao, L., Armus, L., Brandl, B. R., & Charmandaris, V. 2007, ApJ, 654, L49
Sturm, E., et al. 2005, ApJ, 629, L21
Sturm, E., Hasinger, G., Lehmann, I., Mainieri, V., Genzel, R., Lehnert, M. D., Lutz, D., & Tacconi, L. J. 2006, ApJ, 642, 81
Teplitz, H.I., et al. 2006, ApJ, 638, L1
Urry, C.M., & Padovani, P. 1995, PASP, 107, 803
Voshchinnikov, N. V., & Mathis, J. S. 1999, ApJ, 526, 257
Voshchinnikov, N. V., Il'in, V. B., & Henning, Th. 2005, A&A, 429, 371
Voshchinnikov, N. V., Il'in, V. B., Henning, Th., & Dubkova, D. N. 2006, A&A, 445, 167
Voshchinnikov, N. V., & Henning, Th. 2008, A&A, 483, L9
Weedman, D. W., et al. 2005, ApJ, 633, 706
Wooden, D. H., Harker, D. E., Woodward, C. E., Butner, H. M., Koike, C., Witteborn, F. C., & McMurtry, C. W. 1999, ApJ, 517, 1034
Yamamoto, T., Chigai, T., Kimura, H., & Tanaka, H. 2008, Earth, Planets & Space, in press

This paper has been typeset from a TEX/ LATEX file prepared by the author.